Reduction of O_2 to H_2O_2 using Small Polycyclic Molecules[†]

Kristal Lopez,[a] and Michael N Groves[*a]

Hydrogen peroxide is an environmentally friendly oxidizing agent that is important in several industries. It is currently produced industrially via the anthrahydroquinone (AHQ) process where O_2 reacts with a functionalised version of anthrahydroquinone to produce H_2O_2 and anthraquinone. In the previously published DFT pathway for this process the transition of the OOH· radical across the partially dehydrogenated AHQ catalyst was not explored. In this paper, we will use DFT to explore this step and show that there is a deep potential energy minimum that inhibits the OOH· from being fully reduced. We then examine other similar sized polycyclic molecules with two OH-groups on the same side that could serve as alternative catalysts without this issue. In this analysis, we identify Phenanthraquinone as a possible alternative and present the pathway for this candidate to produce H_2O_2 as well as its regeneration with H_2.

1 Introduction

Hydrogen peroxide (H_2O_2) is used in many industries including as a bleaching agent for paper production[1–5] and water treatment[6–8]. Worldwide production exceeds 5.5 million metric tons in 2015 and it continues to climb[3]. It is also used in several other applications including the synthesis of organic chemicals such as Propylene Oxide through the hydrogen peroxide propylene oxide (HPPO) process where hydrogen peroxide is used as the oxidant[9,10]. HPPO is the integration of two processes: first the anthraquinone (AQ) process synthesizes hydrogen peroxide and is then integrated with the propene epoxidation process catalyzed by titanium silicalite[11]. Hydrogen peroxide can also serve as an alternative energy carrier in fuel cell applications. Fuel cells traditionally use oxygen as the oxidant, but in a recent investigation H_2O_2 was used not only as an alternative oxidant but as a reductant making the cell structure simpler[12]. Theoretically, it would provide a higher power output compared to fuel-cells where oxygen is the oxidant.

There are multiple ways under study to synthesize H_2O_2. The $2e^-$ electrochemical processes has recently been gaining in popularity. The focus has been on a water electrolyzer configuration instead of a hydrogen-based fuel cell type system due to the high cost and storage of H_2 gas[13]. In this system, metallic[14–17] and non-metallic[18–22] electrode materials have been studied. A second method to synthesize H_2O_2 is direct synthesis from H_2/O_2 mixtures in a high-pressure gas like CO_2 or N_2. In these cases, a Pd-based catalyst is used and the high-pressure gas is meant to

limit the fire hazard given the explosive nature of H_2/O_2 mixtures as well as the inclusion of methanol as a solvent[13]. Supercritical CO_2 has also been explored as a solvent to replace methanol, however, the reaction temperature plays a significant role. In a study by Landon *et al.* they observed that the critical temperature of CO_2 was high enough to promote a high decomposition rate of H_2O_2. They found that temperatures around 274 K with Pd-Au catalysts and methanol as the solvent results in high yields of H_2O_2[23]. A third method to synthesize hydrogen peroxide is via the gas-phase reaction of a H_2/O_2 non-equilibrium plasma[24,25]. This method has the benefit of not needing any catalysts or added chemicals, however, it does not draw much attention over safety concerns. A double dielectric barrier discharge reactor can safely work with 30 mol% O_2 content[26] which is much higher than the typical 6% explosion limit[27]. A fourth method involves the UV illumination of an aqueous suspension of TiO_2 particles. The efficiency of this photochemical process can be significantly improved with the addition of Cu^{2+}[28]. However, the most common way to synthesize H_2O_2 is via the AQ process[29], which is illustrated in Figure 1. In industry, the majority of H_2O_2 is produced using the AQ process. It consists of two processes: the hydrogenation process and the autoxidation process[29]. H_2O_2 is synthesized in the autoxidation step and the catalyst is regenerated with H_2 on a Pd catalyst to form anthrahydroquinone (AHQ). This process is energy intensive and damages the environment so until a scalable alternative exists it is important to examine and improve the current process to minimize these effects.

In this project, the focus is on the autoxidation step in the AQ process. In the autoxidation step, the triplet O_2 and AHQ produce singlet H_2O_2 and AQ under ambient conditions. In a previous study, density functional theory was used to examine the the autoxidation step of the AQ process[2]. In this work a crucial

[a] California State University, Fullerton, Fullerton, CA, 92831, USA. Fax: +1(657)278-5316; Tel: +1(657)278-7018; E-mail: mgroves@fullerton.edu
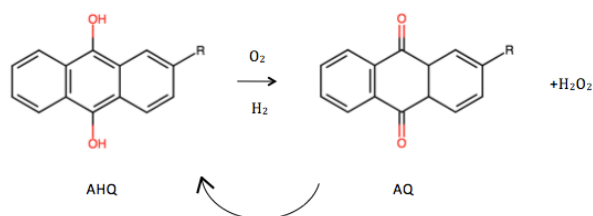
Fig. 1 The overall anthraquinone process. The second half of the reaction is known as the autoxidation step.

step is missing where the hydroperoxyl (OOH·) radical transitions across the partially dehydrogenated AHQ molecule to perform the second hydrogen abstraction. The goal of this investigation is to calculate the transition of the OOH· across the AHQ molecule. It was found that the process has a deep potential well in the singlet state that probably acts as the rate-determining step as the OOH· transitions across the AHQ molecule. Alternative catalysts will be explored with both OH-groups on the same side of the molecule, which eliminates the need for the intermediate to move across the catalyst. Phenanthraquinone has been identified as a promising alternative catalyst, and the barriers of the autoxidation and hydrogenation steps will be presented and compared to those from AHQ to reduce O_2 to H_2O_2.

2 Methods

All calculations are performed using the Python-based density functional theory (DFT) software GPAW [30,31] supported by the Atomic Simulation Environment (ASE) [32]. The generalized gradient approximation (GGA) using the Perdew, Burke, and Ernzerhof (PBE) [33] exchange-correlation functional was used. Dispersion interactions were taken into account using the Tkatchenko-Scheffler method [34]. All reported results use a Monkhorst-Pack $\vec{k}$-point mesh of $2 \times 2 \times 1$, and a grid spacing below 0.1775. Molecular geometries are relaxed to a maximum force less than 0.02 eV/Å. In this project, the O_2 system has a triplet spin, and the H_2O_2 has a singlet spin; therefore, reaction pathways with both spins are calculated. This accomplished by performing spin polarized calculations where the magnetic moment is fixed to 2.0 for triplet state calculations, and 0.0 for the singlet state calculations.

Reaction barriers are calculated between intermediates to find the transition states. The nudged elastic band (NEB) method is used to find minimum energy paths (MEP) [35]. The automated nudged elastic band (AutoNEB) algorithm is an add-on to the basic NEB method that effectively locates transition states because it focuses resources to better characterize less resolved regions along the MEP [36]. The AutoNEB runs with the same basic NEB al-

gorithm, where it will initialize a pathway with a user designated number of images, however, it then iteratively add and relax more images until a predetermined total number of images is achieved. This converges a rough pathway and once the region around the saddle point is resolved, a climbing image is used to converge the transition state [36].

3 Results and discussion

The calculated reaction pathway for reducing O_2 to H_2O_2 is shown in Figure 2. All reported energies for Figure 2 use the separated O_2/AHQ triplet state as the reference. The triplet reaction pathway (purple line) begins with the formation of a hydrogen bond between the O_2 and the AHQ molecule resulting in an energy of -0.11 eV. The first proton transfer to the leading oxygen has a transition state energy of 0.174 eV. After the first hydrogen is transferred, it becomes more favorable for the total spin to reduce to zero as there is an energetic penalty to pick up the second hydrogen in the triplet state. According the the calculations this can occur immediately after the first hydrogen transfer as the singlet and triplet state calculated for this configuration share similar energies (triplet: 0.144 eV; singlet: 0.151 eV). From here, now in the singlet state (gold line), the OOH· rotates around the hydrogen bond formed between it and the partially dehydrogenated AHQ molecule (pAHQ) to present the other O atom towards the other OH-group on the pAHQ molecule. This is a barrierless transition that raises the energy of the system to 0.204 eV. Then the OOH· transitions across the molecule and forms a bond with the carbon adjacent to the other OH-group. The energy of the transition state is 0.53 eV and the resulting intermediate has an energy of -0.795 eV. The energy of the transition state to break this carbon-oxygen bond and transfer the second proton is at 0.16 eV and the energy of the resulting H_2O_2 molecule hydrogen bonded to the dehydrogenated AHQ molecule is -1.068 eV.

The identified location, just after the first proton transfer, is the most likely location for the total spin to reduce from 1 to 0 as there is a convergence in geometry and energy of the two states. Figure S1 in the supplemental information shows an expanded figure where four reaction pathways are illustrated: the two shown in Figure 2, the triplet pathway with the trailing oxygen in the OOH· hydrogenated, and the singlet pathway with the front oxygen in the OOH· hydrogenated. After the identified location where the total spin can relax from 1 to 0 the four pathways diverge in terms of energy and position. Thus it is unlikely that the transition between triplet and singlet states occurs at any other part of the reaction since it would probably involve some sort of electromagnetic emission which has not been previously reported.

Two dashed lines are included in Figure 2 and represent the separated OOH· molecule from the partially dehydrogenated AHQ. Based on these calculations, the reduction of O_2 to H_2O_2 should stay on the same AHQ molecule as it is not energetically favourable for the OOH· radical to separate from the catalyst. This result is inconsistent with a previous description of the AHQ process [28] where they state that this process follows a free-radical chain mechanism [37] that involves two separate AHQ molecules to form H_2O_2. However, in this description the starting catalyst has
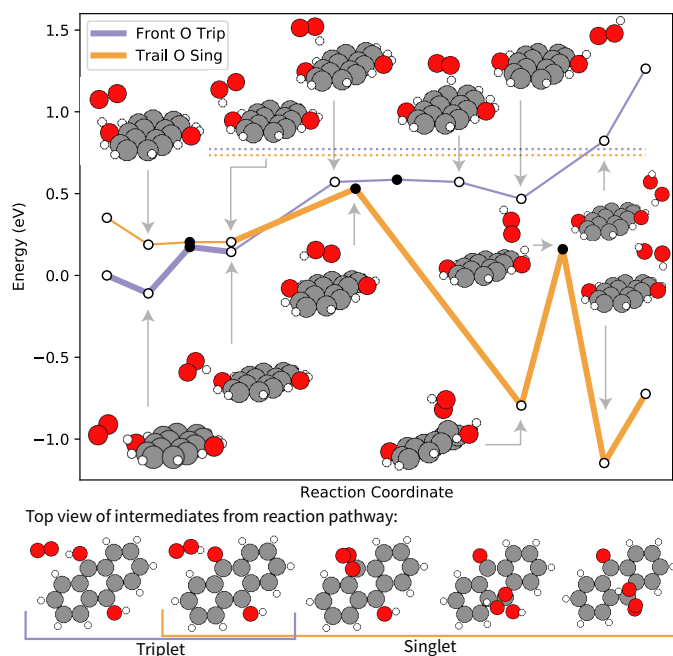
Fig. 2 The most favorable AHQ reaction pathway (outlined with bold lines) calculated for the reduction of O_2 to H_2O_2. Triplet spin calculations are in gold while singlet spin calculations are in purple. The path starts in the triplet state and the first proton is transferred to the O_2 to form OOH·. Then the OOH· reduces its total spin to 0 given that the triplet and singlet states are the same energy in this configuration. Then the OOH· spins to present the unhydrogenated O atom and transitions across the AHQ to eventually become H_2O_2. Intermediates are indicated by the white dots, while transition states are indicated by black dots.

additional hydrogenation at the 9, and 10 position on the ring. In a more recent description of the industrial process[29] it is reported that additional hydrogenation tends to occur at the 5, 6, 7, and 8 position to a much greater degree and results in a less active catalyst than if the anthracene moiety was unsaturated. Given that the calculations included in this work more closely resemble the more recent description of the industrial process, we will conclude that the process involves only one AHQ molecule.

The results reported here are consistent with with the previously reported pathway by Nishimi *et al.*[2] when the difference in the reference state is taken into account. One notable exception is that in this work we were unable to calculate an intermediate where OOH· formed a hydrogen bond with the remaining OH-group in the singlet state. Every attempt resulted in either no association with the OH-group or the formation of H_2O_2. In our case, stable OOH· states were calculated above the partially dehydrogenated AHQ molecule halfway between the C=O and C−OH groups had the same energy as their reported case for the OOH· hydrogen-bonded to the second OH-group. Additionally, the spontaneous formation of H_2O_2 we calculated when we tried to have the OOH· form a hydrogen bond with the second OH-group follows what was presented by Nishimi *et al.* as they also report no transition state.

The major difference between this work and what was presented by Nishimi *et al.* is that along the most favorable pathway presented in Figure 2 is a deep potential well where the OOH·

absorbs on to the carbon atom adjacent to the second OH-group. Nishimi *et al.* reported no information on the transition along the AHQ molecule after the first proton transfer[2]. This calculated pathway serves as an extension to their work and demonstrates that there is a location where the reaction falls into a significant potential energy well. The appearance of this major binding site for the OOH· radical is explained by the same work of Nishimi *et al.* where they identify a molecular orbital at the location of that carbon atom after the first proton transfer that could adsorb the radical as is transitions across the surface.

Given the potential for the OOH· radical in the favorable singlet state to be trapped in a deep potential well during the reaction, a search was performed to determine alternative small carbon-based catalysts that eliminate the need for a potential transit across the catalyst. Twelve alternatives were tested where the two OH-groups, or one OH-group and an acidic C−H (as is the case for Benzo[a]fluorene) located on the same side of the each molecule. These twelve molecules were selected as all of them can exist with hydrogenated and dehydrogenated OH-groups like AHQ and AQ. The results of triplet and single calculations for the hydrogenated catalyst with a separated O_2 molecule and the dehydrogenated catalyst with a separated H_2O_2 molecule are presented in Figure 3.

Based on this search only two molecules present themselves as potential alternatives based on the energy of the singlet state calculation of the dehydrogenated catalyst with a separated H_2O_2 molecule relative to the triplet state calculation of the hydrogenated molecule with a separated O_2 molecule: Phenanthraquinone and Benzo[c]phenantherene. Benzo[c]phenantherene is the only molecule which resulted in an exothermic energy difference. However, when Benzo[c]phenantherene is dehydrogenated one of the oxygen atoms interacts with an adjacent carbon atom to close the ring. It is assumed that this ring closure will not be facile to reopen to regenerate the catalyst so it is disregarded. The other candidate, Phenantrhaquinone, is essentially energetically equivalent for both the separated reactant case and separated product case. However, a similar motif has recently been credited for high electrochemical activity of graphene edges for H_2O_2 synthesis[38].

A full reaction pathway was calculated for the singlet and triplet pathways for the conversion of O_2 to H_2O_2 with Phenanthraquinone. This is illustrated in Figure 4. As before, the system begins in the triplet state and is indicated by the purple line in the figure. All the following energies are relative to the separated O_2 and Phenanthraquinone molecules in the triplet state. The reaction starts by the O_2 molecule forming a hydrogen bond with an OH-group over top of the Phenanthraquinone molecule with an energy of -0.122 eV. The energy of the transition state to transfer the first hydrogen atom is 0.254 eV and the energy of the resulting OOH· radical is 0.145 eV. As the first hydrogen atom transfers the O_2 translates to in front of the Phenanthraquinone molecule. In the singlet state reaction pathway, however, the OOH· molecule remains above the Phenanthraquinone molecule. The shift in position of the OOH· moiety in the triplet state means that there is no early location for the total spin to drop from 1 to 0, like in the AHQ case, as there is no overlap of both energy of the sys-
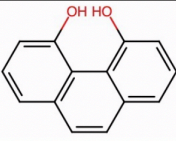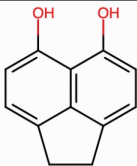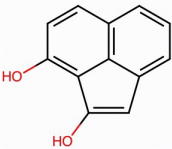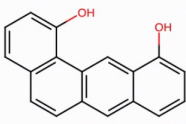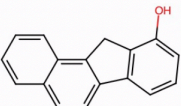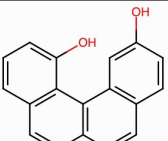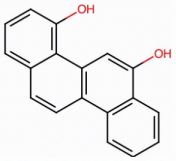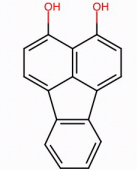
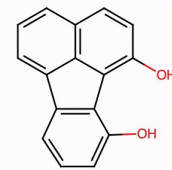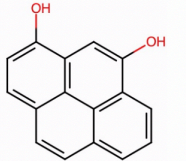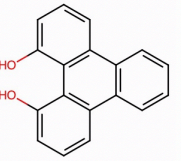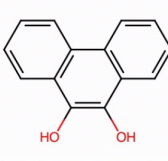|	Phenanthrene	Acenaphthylene (Top)	Acenaphthylene (Side)	Benz[a]anthracene	Benzo[a]fluorene	Benzo[c]phenanthrene
Triplet O_2 (eV)	0	0	0	0	0	0
Singlet O_2 (eV)	0.369	0.369	0.366	0.374	0.376	0.365
Triplet H_2O_2 (eV)	1.573	1.543	1.085	1.183	1.512	1.380
Singlet H_2O_2 (eV)	1.400	1.229	0.760	1.044	0.527	-0.414

	Chrysene	Fluoranthene (Top)	Fluoranthene (Back)	Pyrene	Triphenylene	Phenanthraquinone
Triplet O_2 (eV)	0	0	0	0	0	0
Singlet O_2 (eV)	0.373	0.369	0.377	0.359	0.379	0.363
Triplet H_2O_2 (eV)	1.523	1.514	1.893	1.440	1.574	1.407
Singlet H_2O_2 (eV)	0.865	1.686	1.305	0.319	1.241	0.013

Fig. 3 It is an illustration of the molecules evaluated with the triplet and singlet energies for both the O_2 and H_2O_2 intermediates. Phenanthraquinone was determined to be the most suitable candidate to explore due to the singlet hydrogen peroxide's energy being the closest to zero. All the rest of the evaluated molecules indicated an endothermic reaction, except for benzo[c]phenanthrene. Benzo[c]phenanthreneone was not chosen as the most suitable candidate because it would be difficult to close the catalytic cycle and reduce it so that it would be able to produce more H2O2.

tem and the positions of the molecules until much later in the reaction. This includes the transition states for both the singlet and triplet pathway for the first hydrogen transfer: while they both have similar energies, the molecules are in different places. Moving forward along the reaction pathway, as the OOH begins the second proton transfer, the energy of the triplet and singlet states converge. The blue point on the plot at 0.622 eV illustrates where both the energy and position of both states overlap. From here the total spin of the system can drop to 0 and relax to form H_2O_2 in the singlet state which has an energy of -0.326 eV.

Based on the above reaction pathway, the formation of H_2O_2 is exothermic. Relative to the separated O_2 molecule in the triplet state, the total energy of the system drops to -0.326 eV for the adsorbed H_2O_2 molecule in the singlet state. This is important since this process is driven thermodynamically towards the H_2O_2 production. Furthermore, placing both OH-groups on the same side of the molecule seems to have the intended result where there is no deep intermediate that can kinetically inhibit the reaction.

One interesting result from the above calculated pathway is that H_2O_2 would decompose into singlet O_2. The lowest energy gold (singlet) pathway does not have a point where the energy and position of both molecules in the system overlap with the triplet state pathway. This means that the most favourable reverse reaction would result in singlet O_2 being produced. This result has been observed with carbocatalysts in the literature. The chemiluminescence phenomenon of luminol can be performed with H_2O_2. The accepted pathway involves the decomposition of H_2O_2 into OH and $O_2^{\cdot -}$ radicals resulting in chemiluminescence. Wang *et al.* reported that when this process was catalyzed using graphene oxide[39], and carbon nanodots[40] the H_2O_2 was decomposed into singlet oxygen which lead to chemiluminescence. Wu and Han also report the production of singlet oxygen from H2O2 with hollow fluorescent carbon nanoparticles[41]. All of these reports state that this decomposition follows a route that involves the formation of OH and $O_2^{\cdot -}$ radicals instead of OOH radicals, however, the formation of singlet oxygen from an oxygenated car-
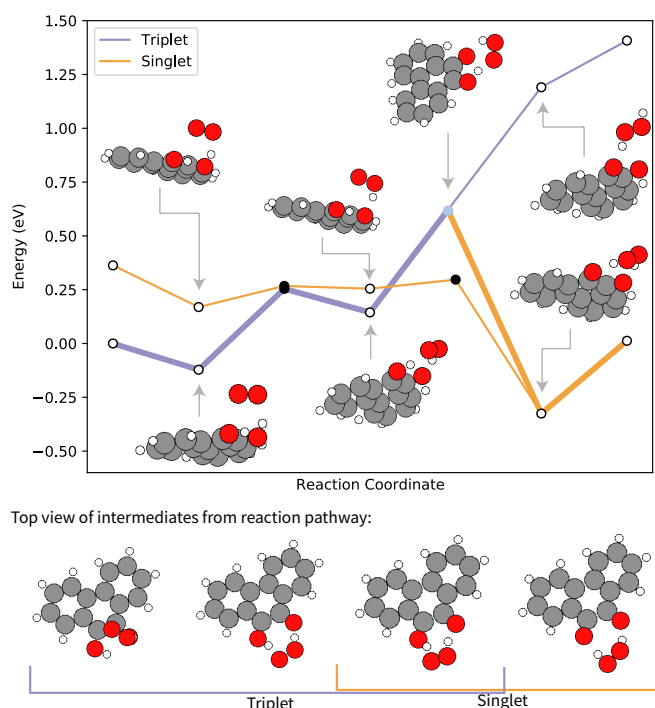
Fig. 4 The triplet and singlet pathways for the conversion of O_2 to H_2O_2 with phenanthraquinone. The purple line is for the triplet pathway, while the gold line is for the singlet pathway. Black and blue circles represent transition states while white circles represent relaxed intermediates.
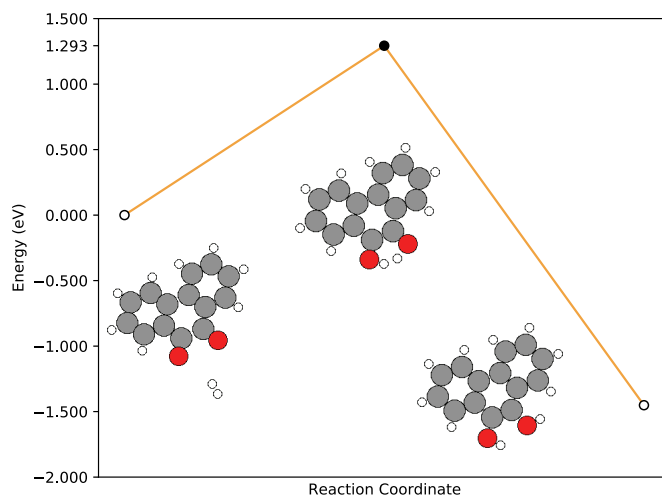

Fig. 5 Reaction pathway for the rehydrogenation of Phenanthraquinone. Black and blue circles represent transition states while white circles represent relaxed intermediates.

bocatalyst provides some support for this calculated pathway.

The hydrogenation step of the AQ catalyst is the most important step in the AQ process[29]. Due to its importance the barrier for the regeneration of dehydrogenated phenanthraquinone was performed. The barrier is 1.293 eV and is illustrated in Figure 5. The pathway begins with the H_2 molecule in front of the two oxygen atoms phenanthraquinone. As the the hydrogen molecule approaches, it separates and the combined system relaxes in to the final form. A second pathway was tested where the H_2 molecule started above the molecule and resulted in an equivalent reaction pathway.

The regeneration of AQ in industrial settings uses a Pd catalyst[29]. This is because the two sites that need to be hydrogenated are distant enough that a catalyst surface is necessary to transport the two hydrogen atoms from H_2 to both sides. A DFT study by Kamachi *et al.* for the rehydrogenation of AQ on Pd(111) surface reported that the barriers for this two-step process are 0.6 eV and 0.7 eV for the first and second hydrogen transfers respectively[42]. The barrier calculated for the regeneration of Phenanthraquinone is significantly larger than these values, however, using a Pd catalyst or an alternative reducing agent could dramatically lower this barrier. The removal of Pd from the process would be a positive step since it must be fully extracted after this catalyst regeneration step as it facilitates the breakdown of H_2O_2 in the O_2 reduction step. An alternative reducing agent might be able to take advantage of simultaneously reducing both oxygen atoms and if that process had a barrier that is comparable to that of the regeneration of AHQ with Pd would dramatically strengthen the case for Phenanthraquinone to be an alternative catalyst for H_2O_2 production. There are many possible degradation products of AQ that result from this regeneration stage, and these should be studied for Phenanthraquinone, especially in the context of different reducing agents, however, this analysis is outside of the scope of this report.

4   Conclusion

This paper presents computational results modeling the transition of OOH· across the AHQ molecule and explore alternative catalysts to eliminate the transition. For the AHQ process, it is favorable for the hydroperoxyl to move across the AHQ molecule and falls into a deep well that will slow down the reaction. Alternative molecules which place OH-groups on the same side of similarly sized molecules were explored to determine if a suitable alternative exists where the O_2 molecule can be fully reduced in the same location. Multiple molecules were surveyed, and phenanthraquinone was selected for further analysis. The reaction barriers for phenanthraquinone were found to be smaller in comparison to those of the AHQ molecule. Regeneration of phenanthraquinone with H_2 had higher barriers than what was previously reported for the reduction of AQ, however, this is without a Pd catalyst that is common to AQ reduction. Being able to reduce phenanthraquinone without the need of a Pd catalyst does present an improvement over the current AQ process since this catalyst must be completely removed so the regenerated catalyst can be used to synthesize H_2O_2.

Conflicts of interest

There are no conflicts to declare.

Acknowledgements

Notes and references

1   N. Sharma, N. K. Bhardwaj and R. B. P. Singh, *J. Cleaner Prod.*, 2020, **256**, 1–11.

2   T. Nishimi, T. Kamachi, K. Kato, T. Kato and K. Yoshizawa, *Eur. J. Org. Chem.*, 2011, **2011**, 4113–4120.

3   R. Ciriminna, L. Albanese, F. Meneguzzo and M. Pagliaro, *ChemSusChem*, 2016, **9**, 3374–3381.

4   X. C. J.-P. C. Xin Tong, Wenhao Shen, *J. Cleaner Prod.*, 2018, **198**, 1066–1075.

5   F. Lopez, M. Diaz, M. Eugenio, J. Ariza, A. Rodriguez and J. L., *Bioresour. Technol.*, 2003, **87**, 255–261.

6   C. Samanta, *Appl. Catal., A*, 2008, **350**, 133–149.

7   W. Wang, X. Lu, P. Su, Y. Li, J. Cai, Q. Zhang, M. Zhou and O. Arotiba, *Chemosphere*, 2020, **259**, 127423.

8   Y. fan Zhang, S. yu Zhang, H. Li, C. wei Wang, F. hao Jiang and J. fu Lyu, *Chemosphere*, 2020, **257**, 127140.

9   F. G. S. R. Teles J.H, Hermans I., *Oxidation*, Wiley, 2015, pp. 11–20.

10 C. Miao, Q. Zhu, Y. Yi, J. Su, N. He, J. Liu and H. Guo, *Ind. Eng. Chem. Res.*, 2019, **58**, 11739–11749.

11 G. Blanco-Brieva, M. Pilar de Frutos-Escrig, H. Martín, J. Campos-Martin and J. Fierro, *Catal. Today*, 2012, **187**, 168–172.

12 S. Fukuzumi, Y. Yamada and K. Karlin, *Electrochim. Acta*, 2012, **82**, 493–511.

13 E. Jung, H. Shin, W. Hooch Antink, Y.-E. Sung and T. Hyeon, *ACS Energy Lett.*, 2020, **5**, 1881–1892.

14 J. S. Jirkovský, I. Panas, E. Ahlberg, M. Halasa, S. Romani and D. J. Schiffrin, *J. Am. Chem. Soc.*, 2011, **133**, 19432–19441.

15 S. Siahrostami, A. Verdaguer-Casadevall, M. Karamad, D. Deiana, P. Malacrida, B. Wickman, M. Escudero-Escribano, E. A. Paoli, R. Frydendal, T. W. Hansen, I. Chorkendorff, I. E. L. Stephens and J. Rossmeisl, *Nat. Mater.*, 2013, **12**, 1137–1143.

16 A. Verdaguer-Casadevall, D. Deiana, M. Karamad, S. Siahrostami, P. Malacrida, T. W. Hansen, J. Rossmeisl, I. Chorkendorff and I. E. L. Stephens, *Nano Lett.*, 2014, **14**, 1603–1608.

17 E. Jung, H. Shin, B.-H. Lee, V. Efremov, S. Lee, H. S. Lee, J. Kim, W. Hooch Antink, S. Park, K.-S. Lee, S.-P. Cho, J. S. Yoo, Y.-E. Sung and T. Hyeon, *Nat. Mater.*, 2020, **19**, 436–442.

18 H. Yang, M. Zhou, W. Yang, G. Ren and L. Ma, *Chemosphere*, 2018, **206**, 439 – 446.

19 H. W. Kim, M. B. Ross, N. Kornienko, L. Zhang, J. Guo, P. Yang and B. D. McCloskey, *Nat. Catal.*, 2018, **1**, 282–290.

20 Z. Lu, G. Chen, S. Siahrostami, Z. Chen, K. Liu, J. Xie, L. Liao, T. Wu, D. Lin, Y. Liu, T. F. Jaramillo, J. K. Nørskov and Y. Cui, *Nat. Catal.*, 2018, **1**, 156–162.

21 C. Xia, S. Back, S. Ringe, K. Jiang, F. Chen, X. Sun, S. Siahrostami, K. Chan and H. Wang, *Nat. Catal.*, 2020, **3**, 125–134.

22 C. Xia, Y. Xia, P. Zhu, L. Fan and H. Wang, *Science*, 2019, **366**, 226–231.

23 P. Landon, P. J. Collier, A. F. Carley, D. Chadwick, A. J. Papworth, A. Burrows, C. J. Kiely and G. J. Hutchings, *Phys. Chem. Chem. Phys.*, 2003, **5**, 1917–1923.

24 J. Zhou, H. Guo, X. Wang, M. Guo, J. Zhao, L. Chen and W. Gong, *Chem. Commun.*, 2005, 1631–1633.

25 Y. Yi, J. Zhou, H. Guo, J. Zhao, J. Su, L. Wang, X. Wang and W. Gong, *Angew. Chem., Int. Ed.*, 2013, **52**, 8446–8449.

26 Y. Yi, J. Zhou, T. Gao, H. Guo, J. Zhou and J. Zhang, *AIChE J.*, 2014, **60**, 415–419.

27 Y. Yi, L. Wang, G. Li and H. Guo, *Catal. Sci. Technol.*, 2016, **6**, 1593–1610.

28 J. M. Campos-Martin, G. Blanco-Brieva and J. L. G. Fierro, *Angew. Chem., Int. Ed.*, 2006, **45**, 6962–6984.

29 G. Goor, J. Glenneberg, S. Jacobi, J. Dadabhoy and E. Candido, in *Hydrogen Peroxide*, American Cancer Society, 2019, pp. 1–40.

30 J. J. Mortensen, L. B. Hansen and K. W. Jacobsen, *Phys. Rev. B*, 2005, **71**, 035109.

31 J. Enkovaara, C. Rostgaard, J. J. Mortensen, J. Chen, M. Dułak, L. Ferrighi, J. Gavnholt, C. Glinsvad, V. Haikola, H. A. Hansen, H. H. Kristoffersen, M. Kuisma, A. H. Larsen, L. Lehtovaara, M. Ljungberg, O. Lopez-Acevedo, P. G. Moses, J. Ojanen, T. Olsen, V. Petzold, N. A. Romero, J. Stausholm-Møller, M. Strange, G. A. Tritsaris, M. Vanin, M. Walter, B. Hammer, H. Häkkinen, G. K. H. Madsen, R. M. Nieminen, J. K. Nørskov, M. Puska, T. T. Rantala, J. Schiøtz, K. S. Thygesen and K. W. Jacobsen, *J. Phys.: Condens. Matter*, 2010, **22**, 253202.

32 A. H. Larsen, J. J. Mortensen, J. Blomqvist, I. E. Castelli, R. Christensen, M. Dułak, J. Friis, M. N. Groves, B. Hammer, C. Hargus, E. D. Hermes, P. C. Jennings, P. B. Jensen, J. Kermode, J. R. Kitchin, E. L. Kolsbjerg, J. Kubal, K. Kaasbjerg, S. Lysgaard, J. B. Maronsson, T. Maxson, T. Olsen, L. Pastewka, A. Peterson, C. Rostgaard, J. Schiøtz, O. Schütt, M. Strange, K. S. Thygesen, T. Vegge, L. Vilhelmsen, M. Walter, Z. Zeng and K. W. Jacobsen, *J. Phys.: Condens. Matter*, 2017, **29**, 273002.

33 J. P. Perdew, K. Burke and M. Ernzerhof, *Phys. Rev. Lett.*, 1996, **77**, 3865–3868.

34 A. Tkatchenko and M. Scheffler, *Phys. Rev. Lett.*, 2009, **102**, 073005.

35 G. Henkelman, B. P. Uberuaga and H. Jónsson, *J. Chem. Phys.*, 2000, **113**, 9901–9904.

36 E. L. Kolsbjerg, M. N. Groves and B. Hammer, *J. Chem. Phys.*, 2016, **145**, 094107.

37 R. A. Sheldon and J. K. Kochi, *Metal-catalyzed Oxidations of Organic Compounds*, Academic Press, 1981, pp. 17 – 32.

38 G.-F. Han, F. Li, W. Zou, M. Karamad, J.-P. Jeon, S.-W. Kim, S.-J. Kim, Y. Bu, Z. Fu, Y. Lu, S. Siahrostami and J.-B. Baek, *Nat. Commun.*, 2020, **11**, 2209.

39 D. M. Wang, Y. Zhang, L. L. Zheng, X. X. Yang, Y. Wang and C. Z. Huang, *J. Phys. Chem. C*, 2012, **116**, 21622–21628.

40 D. M. Wang, M. X. Gao, P. F. Gao, H. Yang and C. Z. Huang, *J. Phys. Chem. C*, 2013, **117**, 19219–19225.

41 Y. Wu and S. Han, *J. Lumin.*, 2016, **179**, 595 – 601.

42 T. Kamachi, T. Ogata, E. Mori, K. Iura, N. Okuda, M. Nagata and K. Yoshizawa, *J. Phys. Chem. C*, 2015, **119**, 8748–8754.

43 J. Towns, T. Cockerill, M. Dahan, I. Foster, K. Gaither, A. Grimshaw, V. Hazlewood, S. Lathrop, D. Lifka, G. D. Peterson, R. Roskies, J. Scott and N. Wilkins-Diehr, *Comput. Sci. Eng.*, 2014, **16**, 62–74.